ELSEVIER

Applied Surface Science 161 (2000) 375–384

applied surface science

www.elsevier.nl/locate/apsusc

Stress-modified electrochemical reactivity of metallic surfaces: atomic force microscopy imaging studies of nickel and alloyed aluminum

J. Hahm, S.J. Sibener *

Department of Chemistry, The James Franck Institute, The University of Chicago, 5640 South Ellis Avenue, Chicago, IL 60637, USA

Received 28 December 1999; accepted 17 February 2000

Abstract

In this paper, we demonstrate that externally applied tensile and compressive stresses can systematically modify the electrochemical surface reactivity of pure and alloyed metals. Atomic force microscopy (AFM) is used to statistically characterize the extent and nature of interface change for nickel and aluminum alloy 2024-T3 subjected to electrochemical conditions under various levels of stress. Statistical analysis of AFM images reveals that the extent of electrochemical reactivity is significantly enhanced when subjecting the sample to tensile as opposed to compressive stress; this enhancement increases monotonically as the level of applied stress is systematically increased. Surface morphologies differ on the pure nickel and alloyed aluminum samples, with the nickel interfaces exhibiting facetted features which are aligned 120° from one another while the surface features on aluminum alloy 2024-T3 are circular pores. These results unambiguously indicate that the kinetics for electrochemical metallic processes, which nucleate at surface defects and grain boundaries, can be significantly modified by the presence of external stress fields.

PACS: 82.65.−i; 82.45.+z; 81.65.Mq; 61.72.Ff; 61.16.Ch; 81.05.Bx; 81.40.Lm
Keywords: Aluminum 2024-T3; Nickel; Stress; Electrochemical reactivity; Atomic force microscopy; Surface chemistry

1. Introduction

Many metals such as aluminum, nickel, and technically important aluminum alloys form self-passivating surface oxide layers which, under ambient conditions, are about 10–20 Å thick. Such passivating layers are of immense importance due to the oxidation protection they offer to bulk materials. These layers are unfortunately vulnerable to breakdown, when exposed to a variety of chemical, electrochemical, and, especially, mechanically stressed environments. One of the most commonly observed degradation phenomena of pure and alloyed metals is pitting.

Pitting corrosion starts by breakdown of the passivating film, providing nucleation sites for etch pits which further develop into corrosion cracking [1] or corrosion fatigue [2]. For example, it has been known that copper content plays an important role in the susceptibility of aluminum–copper alloys such as Al 2024-T3 to corrosion. The chemical reduction of

* Corresponding author. Tel.: +1-773-702-7193; fax: +1-773-702-5863.
E-mail address: s-sibener@uchicago.edu (S.J. Sibener).

0169-4332/00/$ - see front matter
PII: S0169-4332(00)00280-4

copper ions generates nucleation sites that propagate localized corrosion [3]. Extensive experimental and theoretical studies have been done on electrochemical corrosion of metals related to film formation/breakdown mechanisms [4–6]. For example, Schmutz and Frankel [7,8] have studied the corrosion behavior of Al 2024-T3 using scanning Kelvin probe microscopy and in situ atomic force microscopy (AFM). They observed non-uniform dissolution of heterogeneous intermetallic particles in chloride solution, and determined the rates of localized corrosion [7,8].

Understanding corrosion and its prevention is in many ways the lead technical issue in this area of research. For example, anodization of metals is one method of inhibiting localized corrosion. Here, a thick anodic oxide layer frequently serves as a protective coating. Such anodic oxide films are produced by electrochemical oxidative reactions that use an electrolyte that yields the desired oxide layer on top of the metallic substrate [9]. Two types of metal oxide layers, a non-porous barrier layer and a porous oxide layer, can be formed depending on the anodizing conditions, i.e., the applied voltage as well as the type and concentration of the electrolyte [9]. Anodization is of immense technological importance, leading to a vast literature on this subject [9,10]. In spite of this, only a few attempts have been made to collect modern statistical data on such electrochemical metallic reactions, in part due to the difficulties associated with the random locations and sizes of surface features such as porous anodic oxide films [10] and etch pits [11]. In particular, it is difficult to obtain full three-dimensional profiles of these surface characteristics with conventional imaging techniques like scanning electron microscopy (SEM) and transmission electron microscopy (TEM) [12,13]. This is unfortunate as it is important to understand the depth distribution of etch pits as well as the lateral growth area for such features [14]. AFM imaging presents a clear opportunity here, allowing statistical studies of surface morphological evolution to be gathered in a manner that sheds fresh light on the electrochemical reactivity of metallic surfaces.

Another critical issue is to ascertain how, quantitatively, stress and strain fields influence interface structure and reactivity; it is also clear that surface stress is a key factor in explaining many interesting issues pertaining to surface dynamics and surface reconstruction. For example, Swartzentruber et al. [15] employed scanning tunneling microscopy (STM) to study the influence of externally applied stress on the atomic-scale geometry of a Si(001) cantilever beam. They observed reversible asymmetry in the relative populations of the $p(2\times1)$ and $p(1\times2)$ domains, confirming and expanding upon the earlier low energy electron diffraction results of Men et al. [16]. Related studies have been carried out to understand surface chemistry changes under stress and strain [17–20]. Recent efforts have also examined how surface structure and reactivity are influenced by stress [19–22]. Researchers have seen different effects due to tension or compression; this has been done not only for low-index surfaces of fcc metals [21], but also for more complicated bulk samples like NiTi shape memory alloys [22]. It has been shown that steps under tension have larger energies than those under compression on the three low-index surfaces of fcc metals like aluminum [21]. Another recent study involving NiTi alloys reports an asymmetry of stress–strain curves under tension vs. compression, implying the presence of different deformation mechanisms under these two conditions [22]. A creep-rate study of $Al–Al_2O_3$ finds that the minimum creep rate is higher under tension than compression [23]. A molecular dynamics study of aluminum grain boundary diffusion under stress concludes that tensile hydrostatic stress promotes atomic diffusion along grain boundaries while compressive stress inhibits such mobility [24]. The aforementioned studies consistently demonstrate that tension and compression can induce different effects on simple metal structures at the molecular level.

In many real-world applications, the passivating films present on neat and alloyed metals are subjected to increased risk of failure due to simultaneous exposure of the sample to corrosive chemical/electrochemical conditions and stress/strain conditions. An illustrative example would be stress corrosion cracking (SCC), which deals with the combined effects of tension and crack propagation. Due to their obvious importance to the aircraft industry, there have been numerous studies acquired on the SCC of aluminum alloys [25]. Three mechanisms are believed to contribute to this behavior: anodic dissolution, hydrogen-induced cracking, and passive film breakdown [26].

The above discussion emphasizes the need for a modern, systematic examination of how oxidative electrochemical reactions proceed on metallic surfaces when these materials are subjected to varying levels of tensile and compressive stress. In this paper we demonstrate, using AFM, that externally applied stresses can systematically modify the electrochemical reactivity, anodization, of neat and alloyed metals. We do this for samples exposed to a combination of electrochemical and non-equilibrium physical (stress/strain) conditions, examining both the reactivity and the kinetics for such processes. The role that tensile stress plays in accelerating such processes is clearly demonstrated.

2. Experimental procedures and theoretical background

2.1. Procedures for performing electrochemical reactions with externally applied stress

Al 2024-T3 and Ni (99.9% purity) samples were obtained from ESPI (Agoura Hills, CA). Al 2024-T3 was solution heat treated and cold rolled while Ni was first rolled and then annealed at 1000°C. Rectangular sample ''beams'' of Al 2024-T3 and Ni were prepared of dimensions $0.25 \times 2.62 \times 0.01$ in. thick by rinsing sequentially with trichloroethylene, acetone and methanol. A home-built jig with dimensions of $3.5 \times 4 \times 2.25$ in., shown schematically in Fig. 1(a), was used to apply bending stress while simultaneously electrochemically treating the metallic samples. The level of applied stress was always under the yield strength of the sample (unless performing control experiments), i.e., no irreversible deformations were introduced at the stress levels used in our studies. The spatial design of the bending jig allowed us to apply up to 40% of the Al 2024-T3 yield strength, 2×10^4 pounds per square inches (psi), and up to 100% of the pure nickel yield strength, 1.5×10^4 psi. The Al 2024-T3 samples were anodized under bending stress for 2 h using 10% phosphoric acid with an applied DC voltage of 5 V. The pure nickel samples were treated for 2 h in the bending jig arrangement using 0.1 M sulfuric acid and an applied DC voltage of 2 V. These experimental conditions were carefully chosen to yield rates and sufficient

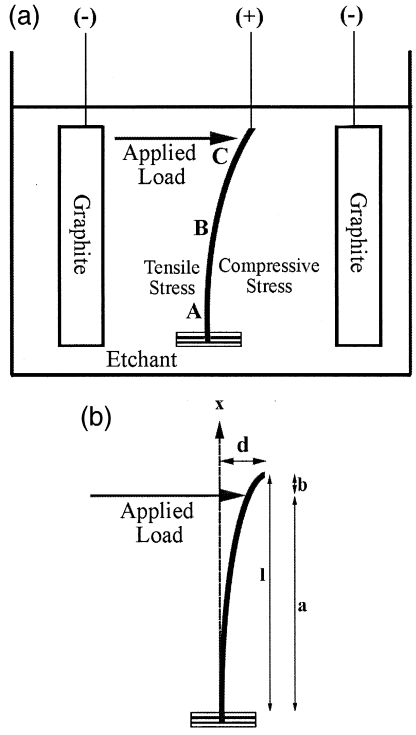

Fig. 1. (a) Illustrative sketch of the electrochemical cell including the home-built cantilever jig for applying bending stress to both sides of a metal sample simultaneously. One side of the sample is under compression while the other side is under tension. In this geometry the sample is subjected to a smoothly varying gradient of stresses which extend out from the fixed point of the jig. Positions A, B, and C illustrate positions along the sample at which electrochemical behavior was monitored under systematically increasing levels of stress; depending on the side of the sample, these positions correspond to varying levels of either compressive or tensile stress. (b) Experimental cantilever geometry for applying bending stress in which the rectangular beam has one end fixed. When a load is applied to the sample, the beam deflects about its initial resting position (x axis). The displacement of the beam, d, is dependent on the applied load.

morphological evolution to occur such that detailed statistical information could be extracted from post-etch AFM imagery. After the electrochemical treatments, the samples were sectioned using a shear cutter. Only the middle areas of the sectioned samples were investigated with AFM, precluding interrogation of areas damaged by the sectioning procedure.

Surface characteristics were imaged with a Topometrix Discoverer AFM using a 75-μm scanner. Statistical data were extracted from a *very* large

set of measurements: for each sample (each experiment) data from 20 different 50×50 μm areas which were subjected to equivalent stresses, i.e., located at the same distance from the fixed point, were typically combined to generate the data for statistical analyses. This bending geometry permitted data for many stress levels to be obtained from one experiment by collecting data at different distances from the jig's fixed point. Moreover, data for compressive and tensile stresses could also be obtained from one experiment by examining data from the opposite sides of the sample. AFM was specifically chosen so that we could interrogate the 3D character of the surface; AFM allows direct measurement of the area, depth, and volume of surface features. This allows a clear picture to be extracted of surface morphological evolution under electrochemical conditions. 2D studies of surface features, for example etch pits, in which only surface etch pit area is analyzed, can be misleading since the size of a very small opening often remains relatively unchanged while etch pit depth increases under the surface [14].

2.2. Stress loading under bending geometries

We have made use of the fact that when a sample develops curvature due to the application of an externally applied force that one side is placed under compressive stress while the opposing side is under tension. The sample is also under varying levels of stress at different distances (x) along the sample depending on the distance from a fixed point. This allows us to collect data at different stress levels by imaging regions that are at varying distances from the fulcrum's fixed point of the jig.

In the bending ''cantilever'' geometry (Fig. 1(b)) the rectangular beam has one fixed end and another free end against which the bending force is applied. This arrangement results in a smooth gradient of applied stress along the length of the beam [27]. The displacement, d, is related to the amount of applied load:

$$d = -w\left(2a^3 - 3a^2(x-b) + (x-b)^3\right)/6EI$$

where w is the applied load, E is the modulus of elasticity, a is the distance from the fixed point to the loading point, and b is the distance from the loading point to the open end of the beam. I is the area moment of inertia which is calculated for a rectangular beam in our experiments using the following formula:

$$I = wt^3/12$$

where w is the beam width and t is the beam thickness. The applied stress can be calculated by measuring the displacement of the beam: $\sigma = Mt/I$ where M is the bending moment defined as $M = -w(x-b)$. The modulus of elasticity of Al 2024-T3 is 10.6×10^6 psi and that of Ni is 30×10^6 psi.

3. Results and discussion

3.1. Control experiments

Control experiments were performed in order to confirm that no systematic bias existed in either the samples themselves (i.e., that sides A and B of each sample behaved the same when electrochemically treated) or that no spatial inhomogeneities existed in our experimental stress-etching cells which might inadvertently influence the kinetics of surface feature formation along the length of the samples. The most basic test was to ensure that no statistically significant physical difference existed between the two sides of a sample. To do this we electrochemically treated an aluminum sample without applying any stress and statistically examined the electrochemical behavior with the AFM. No significant statistical difference was found in either the number of surface features or the total area of surface features between two sides of a given sample. This check was performed on samples taken from each batch of starting material.

The second test was more subtle and, in many ways, more critical for the experiments to follow: using our jig we subjected test samples to bending stresses of up to 34.5% of their yield strength for 2 h. We then eliminated the stresses and proceeded to perform electrochemistry on the samples. The intent here was to convince ourselves that no irreversible changes were introduced in the two opposing surfaces of the sample due to this presumably benign procedure. Again, no statistically meaningful differ-

ences were found either when comparing the electrochemical behavior of sides A and B or when comparing these data to those for a sample that was never stressed. (As a further check, we also intentionally stressed a sample beyond its plastic limit, i.e., subjected it to a load that exceeded its yield strength, thereby introducing permanent change in the sample. In this case a substantial difference was seen in the electrochemical behavior of the compressive vs. tensile stress sides of the test sample. The side subjected to tensile stress side was more prone to electrochemical reaction than was the compressive stress side for such a harshly treated sample. This latter observation has in itself broader implications: it suggests that a deformed metal will exhibit differential electrochemical reactivity on its two opposing surfaces, with what was the tensioned surface of the bent sample being more reactive.)

3.2. Morphology differences between surface features on Al 2024-T3 and Ni

Electrochemically generated pores on Al 2024-T3 samples are round and tend to bunch closely together (Fig. 2(a,b)). For anodizing under standardized conditions (2-h duration, 10% phosphoric acid, bias 5 V DC) the average pore area, depth, and volume typically fell in the following ranges: 14–17 μm^2, 1200–2500 nm, and 17–35 μm^3, respectively. In contrast to this, electrochemically produced surface features on pure Ni look like slits (Fig. 2(c)). Most of these ''slits'' are locally oriented with respect to each other by 120° (Fig. 2(d)). Intergranular bound-

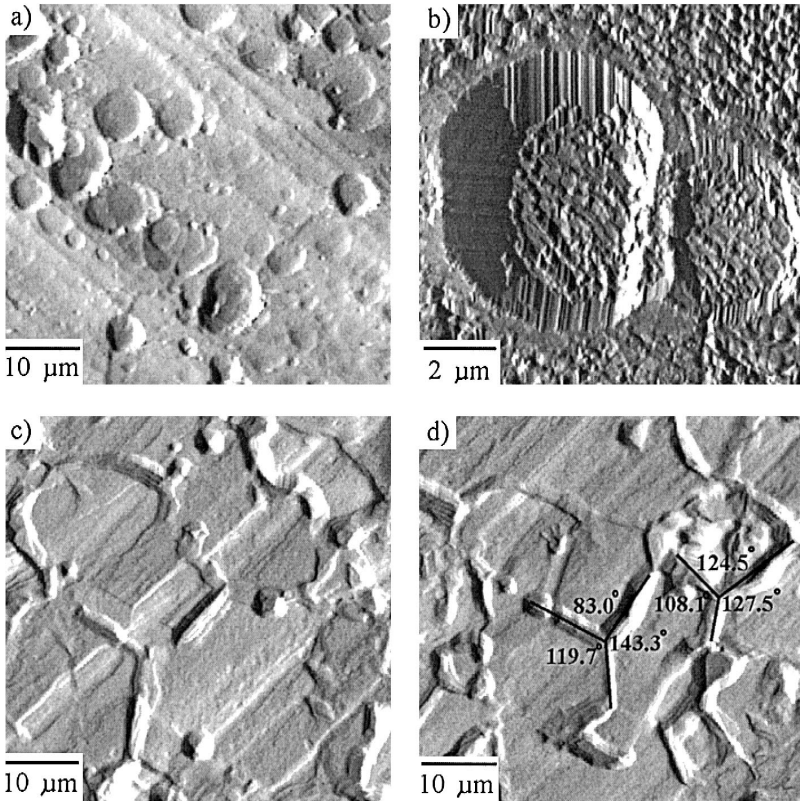

Fig. 2. The 50 × 50 μm (a) and 9.5 × 9.5 μm (b) AFM images of pores on Al 2024-T3 treated in 10% phosphoric acid for 2 h at a bias of 5 V DC. Surface pores on the sample have circular geometry. (c) The 50 × 50 μm AFM image of surface features on Ni in 0.1 M sulfuric acid treated for 2 h at a bias of 2 V DC. (d) Surface features on Ni exhibit facets with neighboring facets oriented 120° with respect to each other; this reflects the underlying grain structure, i.e., polycrystallinity, of the Ni sample.

aries (especially triple junctions) appear to play a particularly important role in the electrochemical process of pure nickel as the reaction paths propagate along such boundaries. Pure nickel grain boundaries have been previously studied in detail in order to categorize grain boundary plane indices and to establish the character of triple junction distributions [28,29].

3.3. Aluminum alloy 2024-T3

Al 2024-T3 was electrochemically anodized while simultaneously being subjected to a gradient of stress levels up to 40% of the material's yield strength. We acquired pore morphology data (area, depth, and volume values) at three different distances from the fixed point of the stress jig. These distances corresponded to externally applied stress levels of 30.7%, 22.1%, and 13.5% of the yield strength; we refer these three regions as areas A, B, C, respectively. These areas are schematically shown in Fig. 1(a). Furthermore, since one side of the sample was under compressive stress and the other tensile stress, we label these two opposing sides as c (compression) and t (tension), respectively. Combined symbols indicate the stress type and magnitude simultaneously, e.g., Bt refers to the specimen area which was under tensile stress at 22.1% of its yield strength. Data from 20 different 50×50 μm areas of Ac, At, Bc, Bt, Cc and Ct zones were used for the analyses that follow.

We shall first examine the data representative of small pores (pore area smaller than 6 μm^2) which reflect the extent of pore initiation, i.e, nucleation. The data shown in Figs. 3 and 4, which represent statistical summaries for pore area and volume, respectively, provide a compelling demonstration that tensile stress systematically enhances the probability of pore formation. Moreover, a subtler trend, visible only in the data for the smallest pores examined, is that compressive stress can actually inhibit the early stages of pore nucleation. We find that the pore statistics between 22.1% and 13.5% of yield strength regions in Figs. 3 and 4 are very similar since the

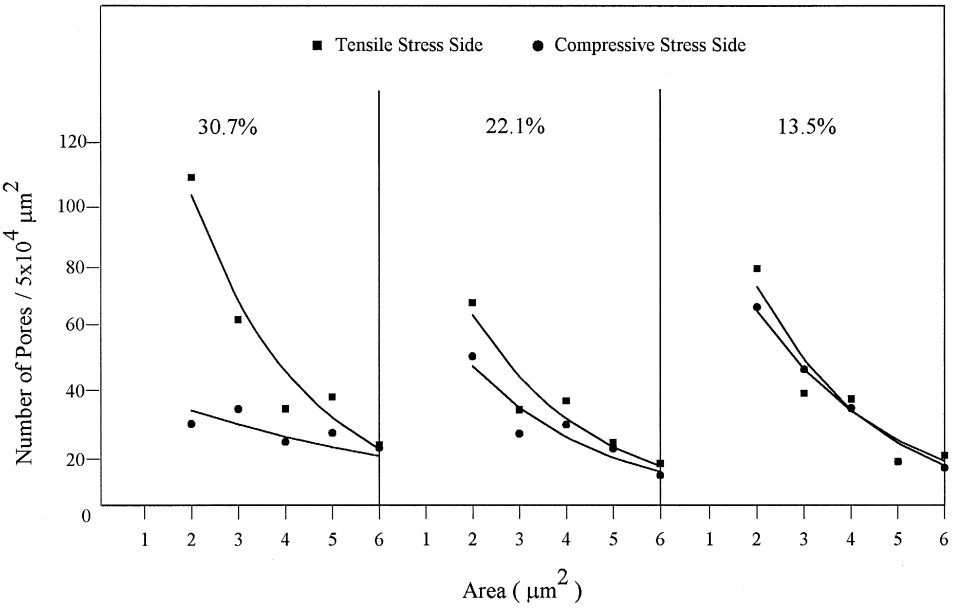

Fig. 3. Pore area histogram of an Al 2024-T3 sample anodized under stress for 2 h in 10% phosphoric acid with a bias of 5 V DC. Three areas corresponding to different stress levels from each side of the sample were imaged with AFM after anodizing; these areas correspond to stress levels of 30.7%, 22.1%, and 13.5% of the material's yield strength. The side under tension has more extensive electrochemical anodization than the side under compression for all levels of applied stress. A more subtle effect is that compressive stress inhibits the formation of small pores, i.e, pore initiation is inhibited by compression. The difference in reactivity between the sides under tension and compression increases monotonically with increasing stress level.

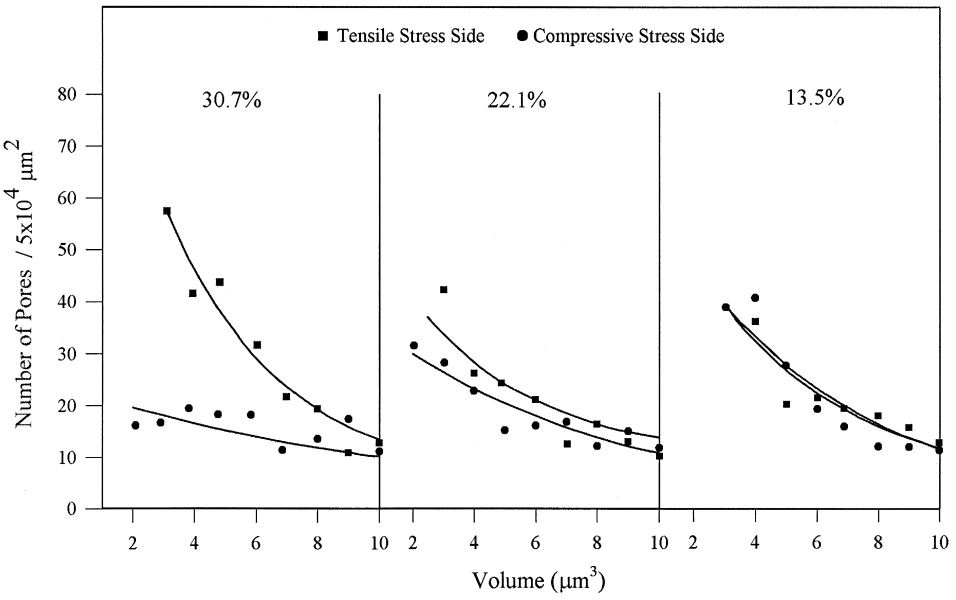

Fig. 4. Pore volume histograms of the electrochemically anodized Al 2024-T3 sample under different levels of externally applied bending stress. These histograms show that the side under tension experiences more extensive electrochemical anodization than the compressed side, perhaps with a threshold, given our resolution, at about 20% of the materials yield strength. The differences in 3D anodization behavior (volume histogram) follow the same trend as seen for the 2D data (area histograms) of Fig. 3; again, the differences in reactivity increase monotonically with increasing stress level.

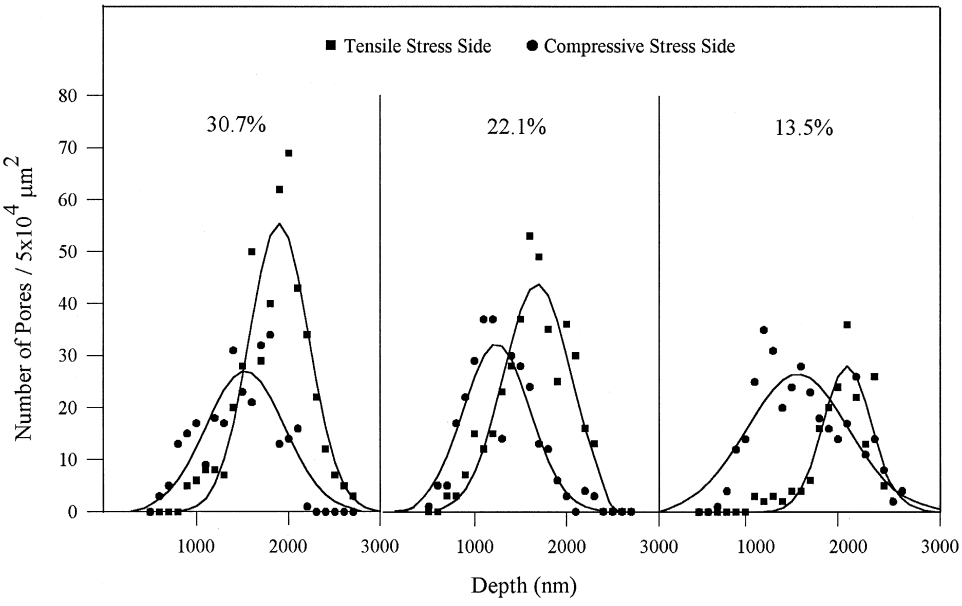

Fig. 5. Pore depth histograms of the electrochemically anodized Al 2024-T3 sample. Electrochemically anodized pores exhibit a Gaussian depth distribution for all stress conditions. Systematic changes as a function of applied stress level are clearly seen (see text for details).

statistics are taken only from the small pores. However, a clear difference between the two stress levels is shown in Fig. 6(a) that reflects the total reacted surface area of the Al 2024-T3. Larger stress levels induce higher electrochemical reactivity of metal surfaces. Previous theoretical and experimental studies suggest similar trends [23,24,30]. Kitagawa et al. [30] studied stress-induced migration via atomic diffusion near aluminum grain boundaries using effective-medium theory. They showed that the diffusion coefficients increase exponentially with tensile strain and decrease with compressive strain. This can be rationalized by noting that in effective medium theory diffusional mobility is linked to the local atomic coordination, and hence potential energy landscape. Jansen et al. also find that creep is faster in tension than in compression [23], and that several different mechanisms can contribute to deformation. They find that the flow of material can take place by dislocation motion, diffusion (vacancy flow or grain boundary sliding), or by cavitation (pore nucleation and growth). These creep experiments suggest two different deformation mechanisms under tension and compression: deformation occurs mainly by cavitation under tension, and by diffusion or dislocation motion under compression. The difference between tension and compression in the aforementioned studies agrees well with the electrochemical behavior differences observed between tension and compression in our experiments.

Fig. 5 gives a more global summary of the data, encompassing pores of all sizes. It provides a good statistical overview of the pore depth distribution from pore initiation (small pores) to growth and coalescence (larger pores). Depth histograms have a Gaussian profile for all the three stress levels. A notable trend is readily apparent: at larger stress levels, the side under tension has a larger number of pores than the side under compression at the peak of the shape distribution. This trend is amplified at higher stress levels. The depth histograms of Fig. 5 also show that a larger number of pores are produced on the tensioned side than the one under compression (perhaps with a threshold, given our resolution, at ca. 20% of the material's yield strength). Fig. 5 also demonstrates, for all stress levels, that the depth distribution is shifted to lower values for compression as compared to tension.

Data that compellingly reinforce the observation that anodization under tension leads to enhanced reactivity vs. compression for Al 2024-T3 are shown in Fig. 6(a). Here we demonstrate that the integrated amount of material removed as a function of stress level varies linearly with applied stress level, with enhanced anodization being systematically observed as a function of tensile loading. No such trend is apparent in the data for compression. Note that the anodizing data for the tensile and compressive data

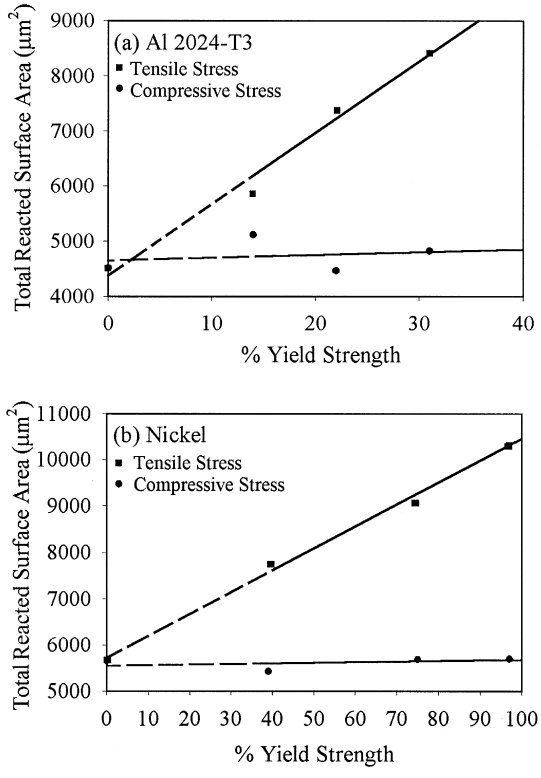

Fig. 6. (a) Total surface area removed for Al 2024-T3 anodized under stress in 10% phosphoric acid for 2 h at a bias of 5 V DC. (b) Total surface area removed for Ni treated in 0.1 M sulfuric acid for 2 h at a bias of 2 V DC. In both cases, electrochemical reactivity on the tensile side is higher than on the compressive side for all stress levels. Solid lines are linear regression fits through the data. Dashed lines show extrapolation of the regression fits extended to zero applied stress; intersection of the compression and tension data sets at zero stress provides an important internal consistency check for these measurements. The reactivity of the side under tension increases linearly as a function of stress level; also note that the reactivity difference between the sides under tension and compression increases monotonically with increasing stress level.

sets, when extrapolated to zero stress level give the same result. This is an important consistency check for our measurements.

Before closing our discussion of Al 2024-T3, we also report on measurements at higher stress levels. These experiments were performed in a different jig, one which had a buckling geometry (two fixed ends which were driven closer to each other) as opposed to the cantilever geometry which was used in all of the previously discussed experiments. This alternate arrangement allowed measurements to be performed up to 74% of the yield strength of this alloy. Electrochemical anodization under these harsher conditions again revealed higher reactivity under tension as compared to compression.

3.4. Pure nickel

Similar experiments were carried out with a nickel sample (99.9% purity) to further elaborate whether externally applied stresses can significantly modify the electrochemical reactivity for other metals. Pure nickel has lower yield strength than Al 2024-T3. Therefore, the same bending jig used in our aluminum alloy studies could be used to apply higher relative stress levels to Ni. We analyzed three regions on each side of the sample with stress levels 97.0%, 74.5%, and 38.6% of nickel's yield strength. Fig. 6(b) displays the results, which again demonstrate a dramatic enhancement of reactivity with applied tensile stress. These data also reveal a linear dependence of overall reactivity as a function of applied stress.

4. Summary

In this paper, we have demonstrated that externally applied tensile and compressive stress fields can significantly modify the oxidative electrochemical surface reactivity of an important engineering alloy, Al 2024-T3, as well as that of Ni. Systematic variation of stress levels was achieved using an in situ cantilever geometry that permitted the simultaneous collection of surface feature data for different levels of tension and compression on the same sample. It was found that moderate tensile stress fields, with magnitudes well below the yield strength of the material, can dramatically accelerate the extent of electrochemical reactivity. A subtler trend was that compressive stress can mildly suppress the formation of small surface features (pores in Al 2024-T3), i.e., pore nucleation is inhibited. AFM images allowed for the acquisition of true 3D statistical data for electrochemically induced changes in surface morphology, i.e., area, depth, and volume of surface features, as well as quantification of the total amount of material removed, as a function of stress level and type. Such data is crucial for elucidating mechanistic details of stress-modified materials' reactivity. Data for the stress-modified electrochemical reactivity of pure nickel were also obtained as part of this study.

The primary finding, supported by an extensive statistical database, is that externally applied stresses can systematically enhance the extent of electrochemical reactivity for these materials. Moreover, this reactivity enhancement increases linearly as a function of applied stress level. The reactivity differences we have delineated in this paper have occurred regardless of sample selection, electrochemical conditions, or method of external stress generation, i.e., our findings are robust, suggesting important fundamental issues that can be addressed in real-world engineering applications to inhibit materials degradation by corrosion.

Acknowledgements

This work was supported by the Air Force Office of Scientific Research via Core and University Research Initiative (AFOSR-URI) funding.

References

[1] S. Berrada, E. Ghali, Can. Metall. Q. 33 (1994) 359.
[2] G. Tu, I.T. Chen, R.Y. Hwang, JSME Int. J., Ser. I 33 (1990) 527.
[3] H. Kaesche, Int. Corros. Conf. Ser. NACE-3 (Localized Corros.) (1974) 516.
[4] F. Mansfeld, Corros. Mech. (1987).
[5] G.M. Scamans, N.J.H. Holroyd, C.D.S. Tuck, Corros. Sci. 27 (1987) 329.
[6] F.F. Fan, A.J. Bard, J. Electrochem. Soc. 136 (1989) 166.
[7] P. Schmutz, G.S. Frankel, J. Electrochem. Soc. 145 (1998) 2285.
[8] P. Schmutz, G.S. Frankel, J. Electrochem. Soc. 145 (1998) 2295.

[9] L. Young, Anodic Oxide Films, Academic Press, New York, 1961.
[10] G.E. Thompson, G.C. Wood, Anodic Oxide Films on Aluminum in ''Treatise on Materials Science and Technology'', Academic Press, New York, 1983, Chap. 5.
[11] N.R. Cawley, D.G. Harlow, J. Mater. Sci. 31 (1996) 5127.
[12] M. Yasuda, F. Weinberg, D. Tromans, J. Electrochem. Soc. 137 (1990) 3708.
[13] M. Yasuda, F. Weinberg, D. Tromans, J. Electrochem. Soc. 137 (1990) 3716.
[14] C. Liao, G.S. Chen, Scr. Mater. 35 (1996) 1341.
[15] B.S. Swartzentruber, Y.W. Mo, M.B. Webb, M.G. Lagally, J. Vac. Sci. Technol., A 8 (1990) 210.
[16] F.K. Men, W.E. Packard, M.B. Webb, Phys. Rev. Lett. 61 (1988) 2469.
[17] M. Schroeder, D.E. Wolf, Surf. Sci. 375 (1997) 129.
[18] D. Sander, H. Ibach, Phys. Rev. B 43 (1991) 4263.
[19] A. Grossmann, W. Erley, H. Ibach, Surf. Sci. 337 (1995) 183.
[20] A.J. Schell-Sorokin, R.M. Tromp, Phys. Rev. Lett. 64 (1990) 1039.
[21] S. Brochard, P. Beauchamp, J. Grilhe, Philos. Mag. Lett. 77 (1998) 125.
[22] Y. Liu, Z. Xie, J.v. Humbeeck, L. Delaey, Acta Mater. 46 (1998) 4325.
[23] A.M. Jansen, D.C. Dunand, Acta Mater. 45 (1997) 4583.
[24] T. Kitamura, Y. Umeno, R. Ohtani, JSME Int. J., Ser. A 41 (1998) 41.
[25] J.P. Fraser, G.G. Elderdge, R.S. Treseder, Corrosion 14 (1958) 37.
[26] T.D. Burleigh, Corrosion 47 (1991) 89.
[27] W. Griffel, Handbook of Formulas for Stress and Strain, Frederick Ungar Publishing, 1996.
[28] L. Priester, D.P. Yu, Mater. Sci. Eng., A 188 (1994) 113.
[29] D. Horton, C.B. Thomson, V. Randle, Mater. Sci. Eng., A 203 (1995) 408.
[30] H. Kitagawa, A. Nakatani, S. Ogata, K. Saitoh, Y. Maegawa, JSME Int. J., Ser. A 40 (1997) 203.